Origin of anomalous strain effects on the molecular adsorption on boron-doped graphene

Joongoo Kang, Yong-Hyun Kim, Greg C. Glatzmaier, and Su-Huai Wei

Citation: The Journal of Chemical Physics **139**, 044709 (2013); doi: 10.1063/1.4816365
View online: http://dx.doi.org/10.1063/1.4816365
View Table of Contents: http://scitation.aip.org/content/aip/journal/jcp/139/4?ver=pdfcov
Published by the AIP Publishing

Origin of anomalous strain effects on the molecular adsorption on boron-doped graphene

Joongoo Kang,[1,a)] Yong-Hyun Kim,[2] Greg C. Glatzmaier,[1] and Su-Huai Wei[1]
[1]*National Renewable Energy Laboratory, Golden, Colorado 80401, USA*
[2]*Graduate School of Nanoscience and Technology, KAIST, Daejeon 305-701, South Korea*

(Received 14 May 2013; accepted 5 July 2013; published online 29 July 2013)

When compressive strain is applied to a single-layered material, the layer generally ripples along the third dimension to release the strain energy. In contrast, such a rippling effect is not favored when it is under tensile strain. Here, using first-principles density-functional calculations, we show that molecular adsorption on boron-doped graphene (BG) can be largely tuned by exploiting the rippling effect of the strained graphene. Under tensile strain, the adsorption energy of K_2CO_3, NO_2, and NH_3 on BG, for which the molecular adsorption is a chemisorption characterized by a covalent B-molecule bond, exhibits a superlinear dependence on the applied strain. In contrast, when microscopic ripples are present in the BG under compressive strain, the adsorption strength is significantly enhanced with increasing the strain. Such a nonlinear and asymmetric effect of strain on the molecular adsorption is a characteristic of two-dimensional systems, because a general elastic theory of molecular adsorption on three-dimensional systems gives a linear and symmetric strain effect on the adsorption strength. We provide the underlying mechanism of the anomalous strain effect on the chemical molecular adsorption on BG, in which the microscopic rippling of the graphene and the creation of the π-dangling bond state near the Dirac point play an important role. Our finding can be used to modify chemical reactivity of graphene with a wide range of application. © *2013 AIP Publishing LLC*. [http://dx.doi.org/10.1063/1.4816365]

I. INTRODUCTION

Graphene,[1] which is a single atomic layer of carbon atoms densely packed in a honeycomb crystal lattice, is an ideal two-dimensional system for studying its unique electronic, magnetic, and mechanical properties. Much of the research on graphene has been directed toward exploration of its novel electronic properties,[2–5] which arise from the unique electronic structure of graphene in which charge carriers behave like massless Dirac fermions. The structural properties of graphene also have been of great interest. At finite temperature, a freestanding graphene sheet can have intrinsic, microscopic corrugations,[6,7] and the rippling can be largely suppressed when the graphene is supported on an atomically flat substrate.[8] Previous scanning tunneling microscopy measurements[9–13] showed that periodic ripples with a wavelength of $\lambda = 2.4$–3.0 nm are created by depositing single-layer graphene on metal surfaces such as iridium and ruthenium. It was also demonstrated that periodic ripples with controlled wavelength and amplitude can be formed by using thermally generated strains.[14] The microscopic or mesoscopic ripples in graphene are responsible for many interesting phenomena in graphene such as strong suppression of weak localization,[15] limited carrier mobility,[16] and gauge-field effect.[17]

The rippling of graphene can be controlled by applying mechanical strain to the sheet.[18] Apart from the intrinsic ripples induced by thermal fluctuations,[6,7] an ideal graphene sheet is atomically flat. Under compressive biaxial strain, the carbon atoms in graphene can relax out of the plane to reduce the strain energy associated with the bond-length change. The deformation in the third dimension induces local curvature in graphene, which tends to increase as the applied strain increases. In contrast, under tensile biaxial strain, the graphene sheet remains flat (thus no curvature exists) because there is no other relaxation mode to keep the C–C bond length less affected. Therefore, the graphene sheet displays an intrinsic asymmetry in the strain-induced local curvature with respect to the sign of strain.

In this paper, using first-principles density-functional calculations, we show that the strain-induced microscopic rippling of graphene leads to anomalous, nonlinear strain effects on the molecular adsorption energy on graphene, provided that the molecular adsorption is a chemisorption in nature that involves the bond breaking of the π-like bonds at the binding site. Most molecules are physisorbed on pristine graphene[19,20] due to the chemically inactive sp^2-bonds in graphene. Thus, for enhanced molecular adsorption beyond physisorption, impurities should be introduced into graphene. In this work, we considered boron-doped graphene, because boron is one electron less than carbon and so the bond is no longer fully saturated.[21–23] B-doped single- or few-layer graphenes (BGs) with a controllable B content have been made by several different methods and strategies.[24–31] For adsorbate, NO_2, NH_3, and carbonate salt (e.g., K_2CO_3) molecules were chosen due to the suitable positions of their highest occupied molecular orbitals (HOMO) for forming a covalent bond with the B site in BG. The adsorption en-

a)Author to whom correspondence should be addressed. Electronic mail: joongoo.kang@nrel.gov

ergy (E_{ads}) of these molecules on BG follows the qualitatively same dependence on the applied strain, which is highly nonlinear and asymmetric with respect to the sign of strain. For the stretched BG under tensile strain, the E_{ads} follows a superlinear dependence on the strain. Under compressive strain, however, the adsorption strength is significantly enhanced, i.e., the strain effect on E_{ads} significantly deviates from the superlinear dependence of strain. Such a nonlinear and asymmetric strain dependence of E_{ads} is unusual, because the strain effect on E_{ads} for physisorption is usually linear and symmetric according to the elastic theory of molecular adsorption. The anomalous strain effect on E_{ads} was also found for the adsorption of F atom on pure graphene, indicating that it is an intrinsic property of graphene derived from its two-dimensionality and the covalent nature of the adsorption. We found that the superlinear dependence of E_{ads} on tensile strain is due to the relatively large reduction of the elastic constant of the host graphene by the chemisorption of an adsorbate. The asymmetric strain effect on E_{ads} arises from the asymmetric strain dependence of the rippling of graphene. The relationship between the local curvature in the microscopic ripples and the adsorption strength will be discussed in details.

II. CALCULATION METHODS

We performed first-principles spin-polarized density functional calculations of molecular adsorption on a single-layer BG under different biaxial strains. Previous experiments[24–29] have shown that the B atoms in BG exist mainly in the form of "graphitic" boron (BC_3) bonding with three carbon neighbors. So, a boron atom in our model is substitutionally doped into the BG. Total energies were calculated within the generalized gradient approximation (GGA-PBE[32]) to the density functional theory (DFT), as implemented in the VASP package.[33] Our DFT calculations employed the projector augmented wave method[34,35] with an energy cutoff of 400 eV for the plane wave part of the wave function. A (10×10) graphene supercell with vacuum separation of 15 Å and a ($3 \times 3 \times 1$) k-point sampling were used in calculations. All atomic forces were minimized to <0.01 eV/Å for a given in-plane strain. The E_{ads} of a molecule (MO) on BG is defined as $E_{ads} = E(\text{BG}) + E(\text{MO}) - E(\text{B*G–MO})$, where E(BG), E(MO), and E(B*G–MO) are the total energies of BG, MO, and the adsorption state B*G–MO, respectively. It is well known that PBE cannot accurately describe dispersion interactions. To verify that the strain effect on E_{ads} does not qualitatively change for the calculations including van der Waals (vdW) interactions, we also performed the non-local vdW density functional (vdW-DF) calculations[36] for K_2CO_3 molecules using optPBE for the exchange functional[37,38] (see Fig. 1). Throughout the paper, the results were obtained by using PBE except if otherwise indicated.

III. RESULTS

A. Physisorption versus chemisorption of K_2CO_3 on graphene

We first compare the molecular adsorptions of K_2CO_3 on unstrained pure graphene and BG. Figures 1(a) and 1(b) show the atomic structures of the physisorbed K_2CO_3 on pure graphene and the chemisorbed K_2CO_3 on BG, respectively. We note that the adsorption of K_2CO_3 on BG pulls out the B atom substantially [Fig. 1(b)], which otherwise lies almost flat in the graphene sheet due to its comparable atomic size with that of carbon. In the protruded geometry (B*G), the B $2p$ orbital becomes more localized toward the protruded side through sp^3-like hybridization [Fig. 2(a)], enhancing the electronic coupling between the B $2p$ orbital and the second HOMO of K_2CO_3 for the covalent B–molecule interaction [Fig. 2(b)]. The bond length of the covalent B–O bond is $d_{B-O} = 1.60$ Å. We found that the E_{ads} of K_2CO_3 on BG is 0.56 eV, which is larger than the E_{ads} on pure graphene ($E_{ads} = 0.39$ eV). Despite the covalent B–O bond, the adsorption strength of K_2CO_3 on BG is still below 1 eV due to the strain energy associated with the adsorption-induced B protrusion. The chemisorption of K_2CO_3 at the B* site breaks the π-like

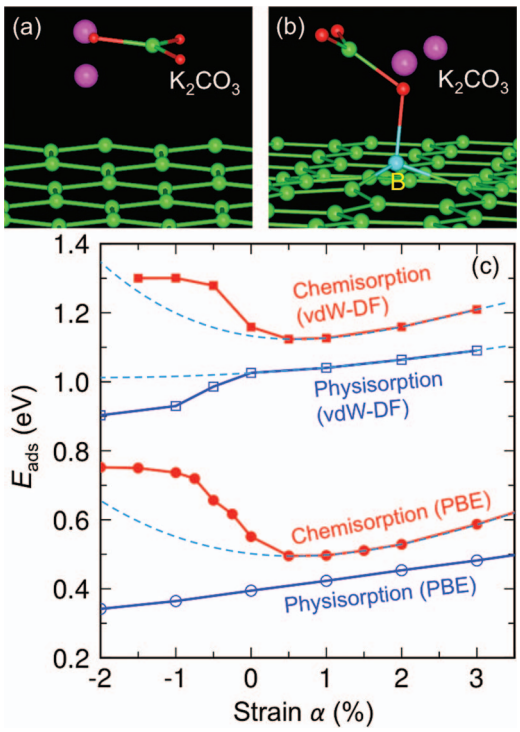

FIG. 1. Physisorption versus chemisorption of K_2CO_3 on graphene. Adsorption geometries of K_2CO_3 on (a) pure graphene and (b) BG. (c) Calculated adsorption energies (E_{ads}) of the physisorption of K_2CO_3 on pure graphene are compared with the E_{ads} of the chemisorption of K_2CO_3 on BG, as a function of strain parameter α (circles for PBE results and squares for vdW-DF calculation results). Negative (positive) α corresponds to compressive (tensile) strain. The dashed curve is the polynomial fittings of E_{ads} for $\alpha > 0$.

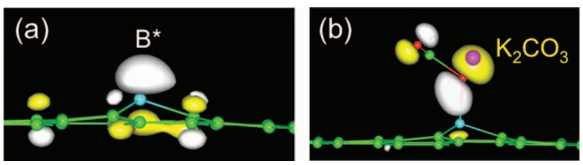

FIG. 2. (a) Side view of the electron wavefunction of the B $2p$-derived state around the protruded boron site (B*) of B*G. The atomic geometry of B*G is taken from the chemisorption geometry B*G–K_2CO_3. (b) The electron wavefunction plot of the bonding state of the covalent B–O bond shows the electronic coupling between the B $2p$ orbital and the second HOMO of K_2CO_3. The electron wavefunctions are obtained at the Γ point.

B–C bonds between the B $2p$ and the neighboring C $2p$ orbitals in BG and this also costs energy (see Sec. IV).

B. Anomalous strain effects on the molecular adsorption on BG

Next, we calculated the E_{ads} of K_2CO_3 on strained pure graphene and BG with the strain parameter $\alpha = (a - a_G)/a_G$, with a and a_G being the cell parameters of the strained and unstrained (10 × 10) graphene supercells, respectively. Our DFT results reveal the following strain effects on E_{ads} that are totally different depending on the adsorption nature of K_2CO_3 [Fig. 1(c)]:

(i) The strain effect on the E_{ads} of K_2CO_3 on pure graphene is almost linear under tensile strain ($\alpha > 0$) for both PBE and vdW-DF calculations, as expected from a simple phenomenological elastic theory[39] of molecular adsorption as follows. When the strain parameter α is small ($\alpha \ll 1$), the total energies E(G) and E(G–MO) for a given lattice parameter a are given by $E(G) = E_o(G) + \beta_G (a - a_G)^2 + O((a - a_G)^3)$ and $E(G–MO) = E_o(G–MO) + \beta_{G–MO} (a - a_{G–MO})^2 + O((a - a_{G–MO})^3)$ for elastic coefficients β_G and $\beta_{G–MO}$. Here, a_G and $a_{G–MO}$ are equilibrium lattice parameters of pure graphene G and G–MO, respectively. Then, the adsorption energy for $a = (1+\alpha)a_G$ is

$$E_{ads}(\alpha) = E_{ads}(0) - 2\alpha\beta_{G–MO}a_G(a_G - a_{G–MO}) + \alpha^2(\beta_G - \beta_{G–MO})a_G^2 + O(\alpha^3).$$

Because the moduli β_G and $\beta_{G–MO}$ are similar for the physisorption of K_2CO_3, the first-order term of α largely determine the strain effect on $E_{ads}(\alpha)$, leading to the near-linear strain dependence of the adsorption strength. The positive slope in the linear strain effect indicates a small lattice expansion after the molecular adsorption (i.e., $a_{G–MO} > a_G$). For PBE results [open circles in Fig. 1(c)], we found the nearly symmetric strain effect with respect to the sign of α, indicating that the strain-induced rippling of pure graphene under compressive strain does not affect much the E_{ads} of K_2CO_3. For vdW-DF results (open squares), however, the adsorption strengths for $\alpha < 0$ are noticeably reduced as compared to the predicted values extrapolated from the linear dependence for $\alpha > 0$. The reduced E_{ads} under compressive strain results from the reduced vdW contact area between K_2CO_3 and the graphene due to the strain-induced rippling.

(ii) The effect of strain on the E_{ads} of K_2CO_3 on BG is, however, highly nonlinear and asymmetric with respect to the sign of the strain parameter α [filled circles or filled squares in Fig. 1(c)]. The same strain dependence of E_{ads} was obtained for both PBE and vdW-DF calculations. According to the simple elastic theory that we explained above, the adsorption energy is given by

$$E_{ads}(\alpha) = E_{ads}(0) - 2\alpha\beta_{B^*G–MO}a_{BG}(a_{BG} - a_{B^*G–MO}) + \alpha^2(\beta_{BG} - \beta_{B^*G–MO}){a_{BG}}^2 + O(\alpha^3).$$

Under tensile strain, the E_{ads} in Fig. 1(c) follows the superlinear dependence on α. The nonlinear effect requires the value $\gamma = |(\beta_{B^*G–MO} - \beta_{BG})/\beta_{BG}|/|(a_{B^*G–MO} - a_{BG})/a_{BG}| \gg 1$, which is the ratio of the relative changes in the elastic coefficient β and the lattice parameter a after the molecular adsorption. For large γ of the order of 100, the second-order term of α becomes as comparable as the first-order term in the above equation and strain range, leading to the superlinear strain dependence of E_{ads}. Indeed, we found that the calculated γ for K_2CO_3 is 200. The relative change of the elastic coefficient is calculated to be −1.7%, while the relative change of the lattice parameter is only −0.008% in our (10 × 10) supercell calculations. On the other hand, under compressive strain with $\alpha < 0$, the adsorption strength of K_2CO_3 is significantly enhanced, i.e., the strain effect on E_{ads} significantly deviates from the superlinear dependence on strain. Therefore, the strain-induced rippling effect should be taken into account for the case of compressive strain.

We found that the anomalous strain effect on the E_{ads} of K_2CO_3 exists regardless of the charge carrier density in BG (Fig. 3). A different carrier density leads to an overall shift of the adsorption energy curve. Furthermore, if a molecule covalently binds to the sp^3-hybridized adsorption site, the nonlinear, asymmetric effect of strain is general, as demonstrated for other molecules such as NO_2 and NH_3 [Fig. 4(a)]. The adsorption geometries of NO_2 and NH_3 on BG are shown in Fig. 5. Our DFT calculations showed that NO_2 adsorbs on the B site through the covalent B–N bond ($d_{B–N} = 1.75$ Å). This adsorption configuration is different from a previous adsorption model[22] in which one of the oxygen atoms of NO_2 bonds to the B site. We found that the adsorption shown here is 0.1 eV more stable than the previously proposed model. Similar to the case of NO_2, NH_3 bonds to the B site, forming a B–N bond with $d_{B–N} = 1.84$ Å. For NH_3, however, the chemisorption is a metastable state with a negative E_{ads}, unless large compressive strain is applied to the BG [Fig. 4(a)].

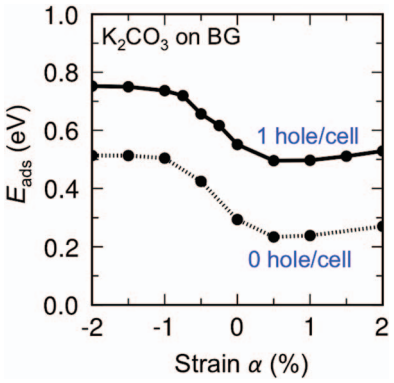

FIG. 3. Comparison of the adsorption energies (E_{ads}) of K_2CO_3 on strained BG for different hole densities. For the BG supercell containing a single B dopant, the hole density is $\sigma_{hole} = 1$ hole/cell. To change σ_{hole} in BG, we added a Li atom to the graphene sheet as an interstitial, which is well separated from the B site. In this case, the hole induced by the B atom in BG:Li is compensated by the electron donated by the Li atom, i.e., $\sigma_{hole} = 0$ hole/cell for BG:Li. The adsorption energy curve for the case of 0 hole/cell is obtained using the formula, $E_{ads} = E(BG:Li) + E(K_2CO_3) - E(BG:Li–K_2CO_3)$.

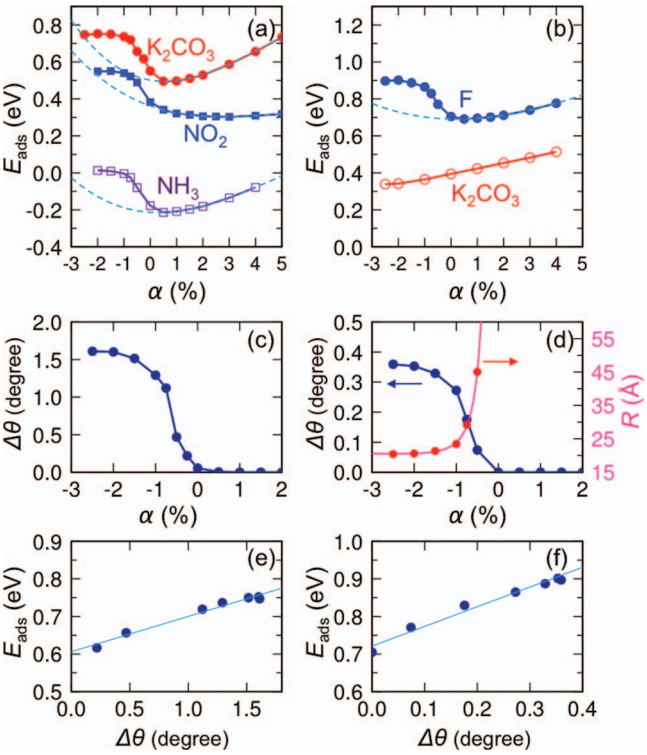

FIG. 4. Effect of the local curvature in graphene on molecular adsorption. (a) Adsorption energy curves of K_2CO_3, NO_2, and NH_3 on BG as a function of strain parameter α. (b) Adsorption energy curves for the chemisorption of F atom and the physisorption of K_2CO_3 on pure graphene. The dashed curves in (a) and (b) are the polynomial fittings of the adsorption energy (E_{ads}) for $\alpha > 0$. (c) The bond-angle deviation $\Delta\theta$, which is proportional to the local curvature K, is shown for BG as a function of α. (d) The strain dependence of $\Delta\theta$ and the radius R of curvature for pure graphene. The relationship between $\Delta\theta$ and E_{ads} for (e) the K_2CO_3 adsorption on BG and (f) the adsorption of F on pure graphene. Solid lines are for eye guiding.

IV. DISCUSSION

Our analysis of the adsorption energy curves for strained BG raises the following important questions in understanding the strain effects on the molecular adsorption on graphene: (1) how does the strain-induced rippling of graphene significantly enhance E_{ads} under compressive strain? (2) What is the microscopic origin of the unusually large ratio $\gamma = |(\beta_{BG} - \beta_{B^*G-MO})/\beta_{BG}|/|(a_{BG} - a_{B^*G-MO})/a_{BG}|$ of the order of 100?

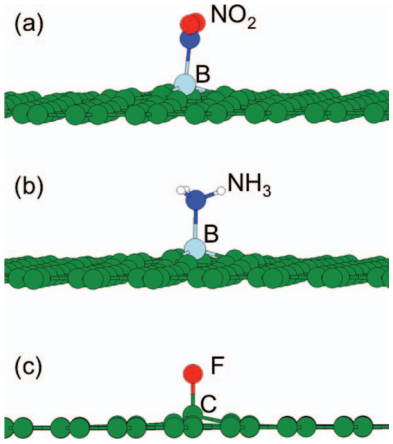

FIG. 5. Atomic structures of (a) NO_2 and (b) NH_3 on unstrained BG and (c) F atom on unstrained pure graphene.

A. Effect of the local curvature in graphene on molecular adsorption

The rippling of graphene under compressive strain generates positive local curvature. In the presence of positive local curvature at the adsorption site, the strain energy associated with the sp^3-like adsorption geometry in B*G–MO becomes reduced. Then, the large deviation of E_{ads} from the superlinear strain dependence for $\alpha < 0$ in Fig. 4(a) can be attributed to the reduced strain energy of B*G–MO due to the positive local curvature. The local curvature effect also exists for pure graphene under compressive strain. So, the nonlinear, asymmetric strain effect demonstrated for B*G–MO can also be found for pure graphene, if the adsorption is a chemisorption in nature. For example, for the adsorption of F atom on pure graphene, the anomalous strain effect on E_{ads} was found as contrary to the linear strain effect for the physisorption of K_2CO_3 [Fig. 4(b)]. The E_{ads} shown in Fig. 4(b) is defined as $E_{ads} = E(G) + E(F_2)/2 - E(G–F)$, where $E(F_2)$ is the energy of a free F_2 molecule. The F atom forms a covalent bond with the protruded C atom [Fig. 5(c)]. (Comprehensive theoretical work on fluorination and chemical functionalization of graphene can be found in, for example, Refs. 40–44.)

To verify the curvature effect on E_{ads}, we analyzed the local curvature in pure graphene as a function of the strain parameter α [Fig. 4(d)]. Here, we first focus on the case where the adsorption site is at the top of a ripple. The site-dependence of the adsorption strength will be discussed in a moment. Then, the Gaussian curvature (K) at the adsorption site is positive and given by $K = 1/R^2$, where R is the radius of curvature. Assuming that the carbon at the top and its three carbon neighbors lie on the sphere of radius R, we can relate the sum of the bond angles (Ω) around the central atom and the R as, $R = \frac{d/2}{\sqrt{1-\frac{4}{3}\sin^2\frac{\Omega}{6}}}$, where d is the C–C distance. Note that for a flat surface, Ω is 360° and thus R diverges. For curved surface, the deviation from the angle 360°, i.e., $\Delta\theta = 360^\circ - \Omega$, is positive, and it is proportional to the curvature K, $\Delta\theta \approx \frac{3\sqrt{3}d^2}{4}K$. In Fig. 4(d), both the R and $\Delta\theta$ are plotted for pure graphene as a function of α. For $\alpha > 0$, the graphene is flat and the R is infinite. The radius R decreases rapidly from infinity to $R = 2.35$ nm as α decreases from 0 to -1%. For $\alpha < -1\%$, however, the R approaches to a minimum value of $R_{min} \approx 2$ nm. Actually, the R_{min} (or K_{max}) in graphene depends on the lateral wavelength (λ) of the ripple. Here, we chose $\lambda \approx 2.5$ nm, which is determined by the supercell size of a (10 × 10) graphene in our DFT calculations. We found that R cannot decrease well below λ. Thus, the $\Delta\theta$ becomes saturated for large compressive strain [Fig. 4(d)]. For BG, the $\Delta\theta$ shows the same strain dependence, although its absolute value is enhanced due to the additional atomic relaxation at around the B site [Fig. 4(c)]. The $\Delta\theta$ (or equivalently K) clearly correlates with the E_{ads}, as shown in Figs. 4(e) and 4(f). This definitely proves the local curvature effect on the enhancement of E_{ads} for $\alpha < 0$. The identified relation

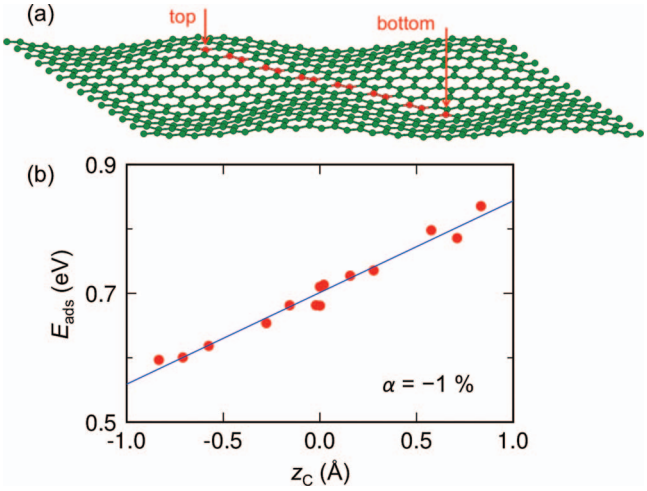

FIG. 6. Site-dependence of the adsorption energy of F atom on the graphene with microscopic ripples. (a) The graphene sheet at $\alpha = -1\%$ is shown with 14 selected adsorption sites (colored in red) including the C atoms at the top and bottom of the ripples. The F atom is assumed to sit on the upper side of the sheet. (b) The calculated adsorption energies (E_{ads}) of F atom as a function of the heights (z_C) of the selected C sites in (a), indicating that F prefers to be adsorbed at the top site. The average height of the whole graphene sheet is set to zero.

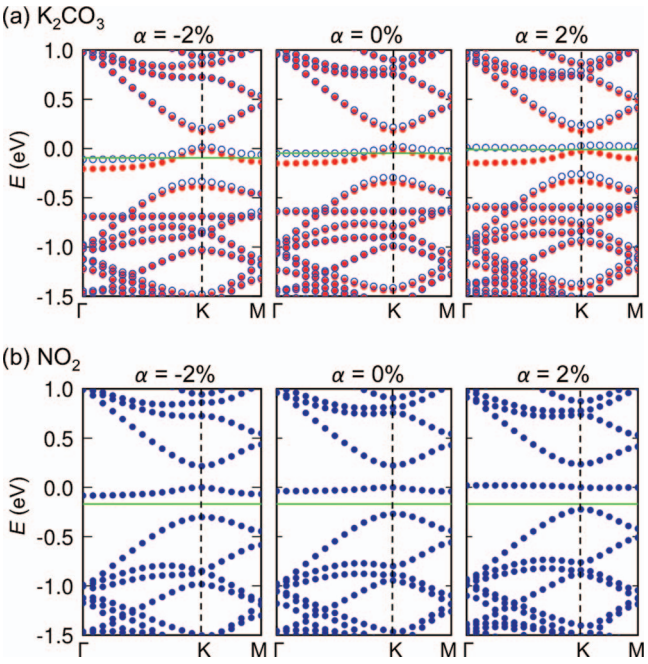

FIG. 7. Calculated electronic band structures of (a) B*G–K_2CO_3 and (b) B*G–NO_2 for different strain parameters α. In (a), the electronic states of the majority spin are shown in filled circles, while the electronic states of the minority spin are shown in open circles. The net magnetic moment depends on α, although the total number of electron in the "zero-energy" dangling-bond states is one for the applied strains: $\mu = 0.56\ \mu_B$ ($\alpha = -2\%$), $0.55\ \mu_B$ ($\alpha = 0\%$), and $0.99\ \mu_B$ ($\alpha = 2\%$). There is no magnetic moment for B*G–NO_2. The horizontal lines in (a) and (b) denote the Fermi level.

between the λ and K_{max} and E_{ads} in this work suggests that one needs to control the wavelength λ of microscopic ripples to be as small as possible in order to largely tune the E_{ads} by strain. Previous work[6,7] showed that the λ of intrinsic ripples in a suspended graphene is about 5–10 nm, which is substantially larger than the wavelength of ripples in our supercell calculations. However, it was experimentally shown that periodic ripples with a wavelength of $\lambda = 2.4$–3.0 nm can be formed by depositing single-layer graphene on metal surfaces such as Ir(111) and Ru(0001).[9–13]

Figure 6 shows how the E_{ads} of F atom on pure graphene depends on the various adsorption sites in the ripples at the strain parameter $\alpha = -1\%$. We selected 14 C atoms [colored in red in Fig. 6(a)] for the adsorption sites, which include the C atoms at the top and bottom of the microscopic ripples. The F atom is assumed to sit on the upper side of the graphene sheet. We found that the calculated E_{ads} correlates well with the height (z_C) of the C adsorption site of the strained pure graphene [Fig. 6(b)]. The maximum E_{ads} is obtained for the top C site, while the adsorption strength is significantly weaker for the bottom C site. At around $z_C = 0$, the E_{ads} is almost the same as the E_{ads} for unstrained graphene.

B. Role of the "zero-energy" dangling-bond state in the molecular chemisorption on graphene

We discuss the microscopic mechanism of the anomalous strain effects on E_{ads}. First, we found that the applied strain in B*G–MO does not create any new electronic state nor leads to any changes in electron occupations of electronic states, as shown for K_2CO_3 and NO_2 in Fig. 7. So, we can exclude the possibility that the anomalous strain effect originates from a qualitative change (e.g., electronic level crossing at a critical strain) in the electronic structure of B*G–MO by strain. Second, we found that the strong covalent B–molecule bond breaks the π-like B–C bonds between the B $2p$ and the neighboring C $2p$ orbitals in BG (Fig. 8). Consequently, the low-energy π electron in B*G–MO behaves as if there is a vacancy at the B site, which generates a "vacancy-induced" localized state in graphene.[45,46] Due to the approximate electron-hole symmetry in BG, the localized π-like dangling-bond (DB) state appears as a relatively flat state at near-zero energy [Figs. 7 and 8(a)]. Figure 8(b) shows a dramatic change in the localized electron wavefunctions around the B site before and after molecular adsorption. Note that there is no electric charge on the B site in the DB state due to the bond breaking effect. We found that the anomalous strain effect exists regardless of the electron occupation of the π dangling-bond state. The π-bond breaking softens the B*G–MO and thus leads to smaller β_{B^*G-MO} than β_{BG}. The noticeable change in β after the molecular adsorption explains the unusually large γ in the elastic theory of molecular adsorption, which is responsible for the quadratic part of the superlinear strain effect on E_{ads} under tensile strain.

In addition to the lattice softening effect, the formation of the zero-energy DB state lowers the electronic energy of the adsorption state by accepting electrons from the high-energy antibonding state of B–molecule [Fig. 8(a)]. This electronic energy gain (E_{elec}), which is larger than the energy cost (E_{strain}) associated with the strains in the σ-like B–C bonds at the protruded B* site, stabilizes the adsorption of molecules on the B site. The adsorption-induced breaking of the π-like B–C bonds also costs the bond-breaking energy E_{bb}. Hence, the adsorption strength is determined by the

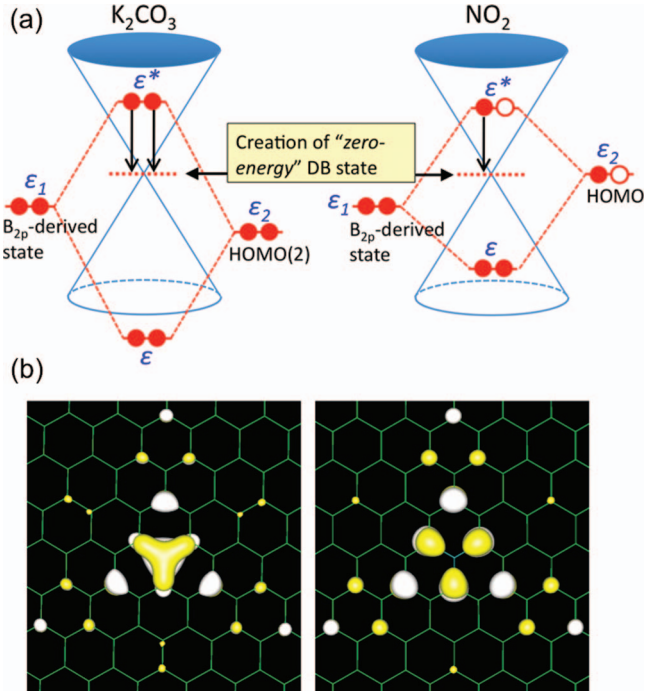

FIG. 8. Mechanism of molecular adsorption on BG. (a) Electronic coupling model for the covalent interaction of B 2*p*-derived localized state ε_1 and a molecular sate ε_2 for K_2CO_3 (left) and NO_2 (right). (b) The adsorption-induced change in the localized electron wavefunction around the B site in BG; the B 2*p*-derived state ε_1 of B*G before the molecular adsorption (left) and the "zero-energy" dangling-bond (DB) state that is created by the adsorption of K_2CO_3 (right). The electron wavefunctions are obtained at the Γ point.

competition among these energy components as, $E_{ads} = E_{elec} - E_{strain} - E_{bb}$. Both E_{strain} and E_{bb} are reduced in the presence of the positive local curvature K around the adsorption site, leading to the significant enhancement of E_{ads} under compressive strain.

V. SUMMARY AND CONCLUSIONS

Using first-principles DFT calculations, we reveal the qualitatively different effects of strain on the molecular adsorption energy on pure or modified graphene, depending on the nature of the molecular adsorption. For physisorption (e.g., K_2CO_3 on pure graphene), the adsorption strength follows a linear dependence on the strain, which is "normal" according to the standard elastic theory of molecular adsorption. In contrast, for chemisorption (e.g., K_2CO_3 on BG), the strain dependence of E_{ads} is highly nonlinear and asymmetric with respect to the sign of strain; (i) under tensile strain, the E_{ads} exhibits a superlinear dependence on the strain due to the relatively large reduction of the elastic constant of the host graphene by the chemisorption of an adsorbate. The softening of the graphene is caused by the bond breaking of the π-like bonds at the adsorption site. (ii) Compressive biaxial strain generally leads to the rippling in graphene. The strain-induced local curvature around the adsorption site substantially reduces the strain energy associated with the sp^3-like chemisorption geometry of the adsorption site. As a result, the adsorption strength is significantly enhanced by compressive strain, when the lateral dimension λ of the microscopic ripples is sufficiently small (λ < 5 nm). Thus, our finding suggests that the combined approach of impurity doping and strain engineering of graphene provides a feasible way to modify the chemical activity of graphene.

ACKNOWLEDGMENTS

We thank A. K. Starace for discussions. This work was funded by the NREL LDRD program (DE-AC36-08GO28308). This research used capabilities of the NREL CSC (DE-AC36-08GO28308) and the NERSC (DE-AC02-05CH11231). Y.-H.K. was supported by the National Research Foundation of Korea (NRF) grants (2012-046191) and the Global Frontier R&D Program by the Center for Multiscale Energy Systems (2011-0031566) of Korea government (MSIP).

[1]K. S. Novoselov, A. K. Geim, S. V. Morozov, D. Jiang, Y. Zhang, S. V. Dubonos, I. V. Grigorieva, and A. A. Firsov, Science **306**, 666–669 (2004).
[2]K. S. Novoselov, A. K. Geim, S. V. Morozov, D. Jiang, M. I. Katsnelson, I. V. Grigorieva, S. V. Dubonos, and A. A. Firsov, Nature (London) **438**, 197–200 (2005).
[3]Y. Zhang, Y.-W. Tan, H. L. Stormer, and P. Kim, Nature (London) **438**, 201–204 (2005).
[4]C.-H. Park, L. Yang, Y.-W. Son, M. L. Cohen, and S. G. Louie, Nature Phys. **4**, 213–217 (2008).
[5]A. H. Castro Neto, F. Guinea, N. M. R. Peres, K. S. Novoselov, and A. K. Geim, Rev. Mod. Phys. **81**, 109 (2009).
[6]J. C. Meyer, A. K. Geim, M. I. Katsnelson, K. S. Novoselov, T. J. Booth, and S. Roth, Nature (London) **446**, 60–63 (2007).
[7]A. Fasolino, J. H. Los, and M. I. Katsnelson, Nature Mater. **6**, 858–861 (2007).
[8]C. H. Lui, L. Liu, K. F. Mak, G. W. Flynn, and T. F. Heinz, Nature (London) **462**, 339–341 (2009).
[9]A. T. N'Diaye, S. Bleikamp, P. J. Feibelman, and T. Michely, Phys. Rev. Lett. **97**, 215501 (2006).
[10]S. Marchini, S. Günther, and J. Wintterlin, Phys. Rev. B **76**, 075429 (2007).
[11]B. Wang, M.-L. Bocquet, S. Marchini, S. Günther, and J. Wintterlin, Phys. Chem. Chem. Phys. **10**, 3530 (2008).
[12]A. L. Vázquez de Parga, F. Calleja, B. Borca, M. C. G. Passeggi, Jr., J. J. Hinarejos, F. Guinea, and R. Miranda, Phys. Rev. Lett. **100**, 056807 (2008).
[13]M. Roos, D. Künzel, B. Uhl, H.-H. Huang, O. B. Alves, H. E. Hoster, A. Gross, and R. J. Behm, J. Am. Chem. Soc. **133**, 9208–9211 (2011).
[14]W. Bao, F. Miao, Z. Chen, H. Zhang, W. Jang, C. Dames, and C. N. Lau, Nat. Nanotechnol. **4**, 562–566 (2009).
[15]S. V. Morozov, K. S. Novoselov, M. I. Katsnelson, F. Schedin, L. A. Ponomarenko, D. Jiang, and A. K. Geim, Phys. Rev. Lett. **97**, 016801 (2006).
[16]S. V. Morozov, K. S. Novoselov, M. I. Katsnelson, F. Schedin, D. C. Elias, J. A. Jaszczak, and A. K. Geim, Phys. Rev. Lett. **100**, 016602 (2008).
[17]F. Guinea, B. Horovitz, and P. Le Doussal, Phys. Rev. B **77**, 205421 (2008).
[18]S. Cho, S. D. Kang, W. Kim, E.-S. Lee, S.-J. Woo, K.-J. Kong, I. Kim, H.-D. Kim, T. Zhang, J. A. Stroscio, Y.-H. Kim, and H.-K. Lyeo, Nature Mater. (in press); e-print arXiv:1305.2845.
[19]T. O. Wehling, K. S. Novoselov, S. V. Morozov, E. E. Vdovin, M. I. Katsnelson, A. K. Geim, and A. I. Lichtenstein, Nano Lett. **8**, 173–177 (2008).
[20]O. Keenaerts, B. Partoens, and F. M. Peeters, Phys. Rev. B **77**, 125416 (2008).
[21]Y.-H. Kim, Y. Zhao, A. Williamson, M. J. Heben, and S. B. Zhang, Phys. Rev. Lett. **96**, 016102 (2006).
[22]J. Dai, J. Yuan, and P. Giannozzi, Appl. Phys. Lett. **95**, 232105 (2009).
[23]Y. Zhao, L. Yang, S. Chen, X. Wang, Y. Ma, Q. Wu, Y. Jiang, W. Qian, and Z. Hu, J. Am. Chem. Soc. **135**, 1201–1204 (2013).
[24]L. S. Panchakarla, K. S. Subrahmanyam, S. K. Saha, A. Govindaraj, H. R. Krishnamurthy, U. V. Waghmare, and C. N. R. Rao, Adv. Mater. **21**, 4726–4730 (2009).
[25]T. Wu, H. Shen, L. Sun, B. Cheng, B. Liu, and J. Shen, New J. Chem. **36**, 1385–1391 (2012).

[26]X. Li, L. Fan, Z. Li, K. Wang, M. Zhong, J. Wei, D. Wu, and H. Zhu, Adv. Energy Mater. **2**, 425–429 (2012).
[27]Z.-H. Sheng, H.-L. Gao, W.-J. Bao, F.-B. Wang, and X.-H. Xia, J. Mater. Chem. **22**, 390 (2012).
[28]Y.-B. Tang, L.-C. Yin, Y. Yang, X.-H. Bo, Y.-L. Cao, H.-E. Wang, W.-J. Zhang, I. Bello, S.-T. Lee, H.-M. Cheng, and C.-S. Lee, ACS Nano **6**, 1970–1978 (2012).
[29]M. Endo, T. Hayashi, S.-H. Hong, T. Enoki, and M. S. Dresselhaus, J. Appl. Phys. **90**, 5670 (2001).
[30]Y. A. Kim, K. Fujisawa, H. Muramatsu, T. Hayashi, M. Endo, T. Fujimori, K. Kaneko, M. Terrones, J. Behrends, A. Eckmann, C. Casiraghi, K. S. Novoselov, R. Saito, and M. S. Dresselhaus, ACS Nano **6**, 6293 (2012).
[31]T. Lin, F. Huang, J. Liang, and Y. Wang, Energy Environ. Sci. **4**, 862–865 (2011).
[32]J. P. Perdew, K. Burke, and M. Ernzerhof, Phys. Rev. Lett. **77**, 3865–3868 (1996).
[33]G. Kresse and J. Furthmüller, Phys. Rev. B **54**, 11169–11186 (1996).
[34]P. B. Blöchl, Phys. Rev. B **50**, 17953 (1994).
[35]G. Kresse and D. Joubert, Phys. Rev. B **59**, 1758 (1999).
[36]M. Dion, H. Rydberg, E. Schröder, D. C. Langreth, and B. I. Lundqvist, Phys. Rev. Lett. **92**, 246401 (2004).
[37]J. Klimeś, D. R. Bowler, and A. Michaelides, J. Phys. Condens. Matter **22**, 022201 (2010).
[38]J. Klimeś, D. R. Bowler, and A. Michaelides, Phys. Rev. B **83**, 195131 (2011).
[39]J. Zhu, F. Liu, G. B. Stringfellow, and S.-H. Wei, Phys. Rev. Lett. **105**, 195503 (2010).
[40]O. Leenaerts, H. Peelaers, A. D. Hernández-Nieves, B. Partoens, and F. M. Peeters, Phys. Rev. B **82**, 195436 (2010).
[41]D. W. Boukhvalov and M. I. Katsnelson, J. Phys.: Condens. Matter **21**, 344205 (2009).
[42]D. W. Boukhvalov, Phys. Chem. Chem. Phys. **12**, 15367–15371 (2010).
[43]H. Xiang, E. Kan, S.-H. Wei, M.-H. Whangbo, and J. Yang, Nano Lett. **9**, 4025–4030 (2009).
[44]B. Huang, H. Xiang, Q. Xu, and S.-H. Wei, Phys. Rev. Lett. **110**, 085501 (2013).
[45]V. M. Pereira, F. Guinea, J. M. B. Lopes dos Santos, N. M. R. Peres, and A. H. Castro Neto, Phys. Rev. Lett. **96**, 036801 (2006).
[46]E. V. Castro, M. R. Lopés-Sancho, and M. A. H. Vozmediano, Phys. Rev. Lett. **104**, 036802 (2010).